

expansion ratios. Their measurements showed that a decrease in the aspect and expansion ratio has a stabilizing effect which extends the range of Reynolds numbers over which symmetric flow can exist.

Fearn *et al.* (1990) presented an experimental and numerical investigation of 1:3 sudden planar expansion. They found that $Re_{cr} = 40.45$ with Re based on the channel's upstream half height and maximum inlet velocity. There have also been considerable numerical investigations of sudden expansion flow. Battaglia *et al.* (1997) and Drikakis (1997) studied numerically the effect of the channel expansion ratio on the symmetric and asymmetric flow in two-dimensional channels. They found that the critical Reynolds number decreases with increasing channel expansion ratio. At a fixed supercritical Reynolds number, the location at which the jet first impinges on the channel wall grows with the expansion ratio. Chiang *et al.* (2000) performed many computational investigations in order to study the side-wall effect on a fluid flow downstream of a channel expansion which is plane. The expansion ratio under investigation is 3 and the aspect ratios in the range of 3 to 48, in the three-dimensional analyses. Their results show that a decrease in aspect ratio has a stabilizing effect. Schreck and Schäfer (2000) report the same observation. This confirms the experimental observation of Cherdron *et al.* (1978).

De Zilwa *et al.* (2000) have developed a calculation method to represent flows downstream of plane symmetric expansions with dimensions and velocities encompassing laminar and turbulent flows. Their results show that for laminar flow, the increase of the separating boundary layer thickness leads to longer regions of separation and no dominant frequency for Reynolds numbers up to those at which the third separation region was observed. Jotkar *et al.* (2015) have studied the linear instability mechanisms of two-dimensional flows through straight-diverging channels with variable angle of divergence α , and expansion ratio (1:2 and 1:3). The results show that the two critical Reynolds number values are affected by the expansion ratios and the angle of divergence.

For non-Newtonian fluids, Mishra and Jayaraman (2002) have used a continuation method with a finite element grid and a geometric perturbation to compute two successive symmetry-breaking flow transitions with increasing Reynolds number in flow of generalized Newtonian fluids through a 1:16 sudden planar expansion. The results show that when the extent of shear-thinning is increased (lower n), the onset Reynolds number increases and the predicted extent of pressure recovery lowers. Neofytou and Drikakis (2003) employed three non-Newtonian models (Casson, Power-Law, and Quemada model), to investigate the instabilities occurring in flow through a 1:2 sudden expansion. The computations reveal that similar to Newtonian fluid flow through a suddenly expanded channel, instability also occurs in non-Newtonian fluids flow. The instability is manifested by a symmetry

breaking of the flow separation. The onset of the instability depends on the specific parameters involved in each model's constitutive equation.

Oliveira (2003) studied numerically the flow of viscoelastic liquids with constant shear viscosity through a symmetric 1:3 planar sudden expansion for a range of Reynolds numbers from 0 to 100. The constitutive model used follows the modified FENE-CR equation (valid for relatively dilute solutions of polymeric fluids). They found that the elasticity effect is to delay the onset of the bifurcation and reduce the degree of flow asymmetry. Manica and De Bortoli (2004) offered a numerical solution of incompressible laminar flows through a channel with 1:3 sudden expansion for Power-Law fluids. Results show that bifurcations occur for the range of Power-Law index $0.2 \leq n \leq 2$. For shear-thinning fluids, the second bifurcation appears after that of the Newtonian situation while the opposite occurs for shear-thickening. Ternik *et al.* (2006) studied numerically the flow of non-Newtonian fluid through a planar symmetric 1:3 sudden expansion in order to obtain the critical Reynolds number values. The Quadratic model is employed to accommodate the shear-thickening behaviour. The results indicate that the shear-thickening behaviour lowers the threshold of the transition from flow symmetry to its asymmetry and increases the reattachment length.

Neofytou (2006) numerically investigated the effects of attributes of generalized Newtonian fluids on the threshold of transition from symmetry to asymmetry flow through a symmetric 1:2 sudden expansion. The study included both shear-thinning and shear-thickening fluids covering a range of Power-Law model indices from 0.3 to 3 whereas shear-thinning effects were investigated also with the use of the Casson model. Their results show that for both Power-Law and Casson models, the critical Re_g of transition from symmetry to asymmetry is linearly related to the dimensionless shear rate at the wall. Ternik (2009) investigated the effect of the generalized Newtonian fluids on the threshold of the transition from flow symmetry to its asymmetry for the flow through a 1:3 planar sudden expansion. He considered purely viscous shear-thinning fluids using the Power-Law model for $n = 0.6$ and 0.8 , and compare them with the Newtonian fluid ($n = 1.0$) in the range of generalized Reynolds number $10 \leq Re_g \leq 150$. Results indicate that the shear-thinning viscous behaviour increases the onset of bifurcation phenomena and the critical value of Reynolds number.

Recently, Dhinakaran *et al.* (2013) used a finite volume method to investigate numerically the laminar flow of inelastic non-Newtonian fluids obeying the Power-Law model through a 1:3 planar sudden expansion. A broad range of Power-Law indices ($0.2 \leq n \leq 4$) and generalized Reynolds numbers ($0.01 \leq Re_g \leq 600$) was considered. They found that the shear-thinning behaviour increases the critical Re_g , while shear-thickening has the

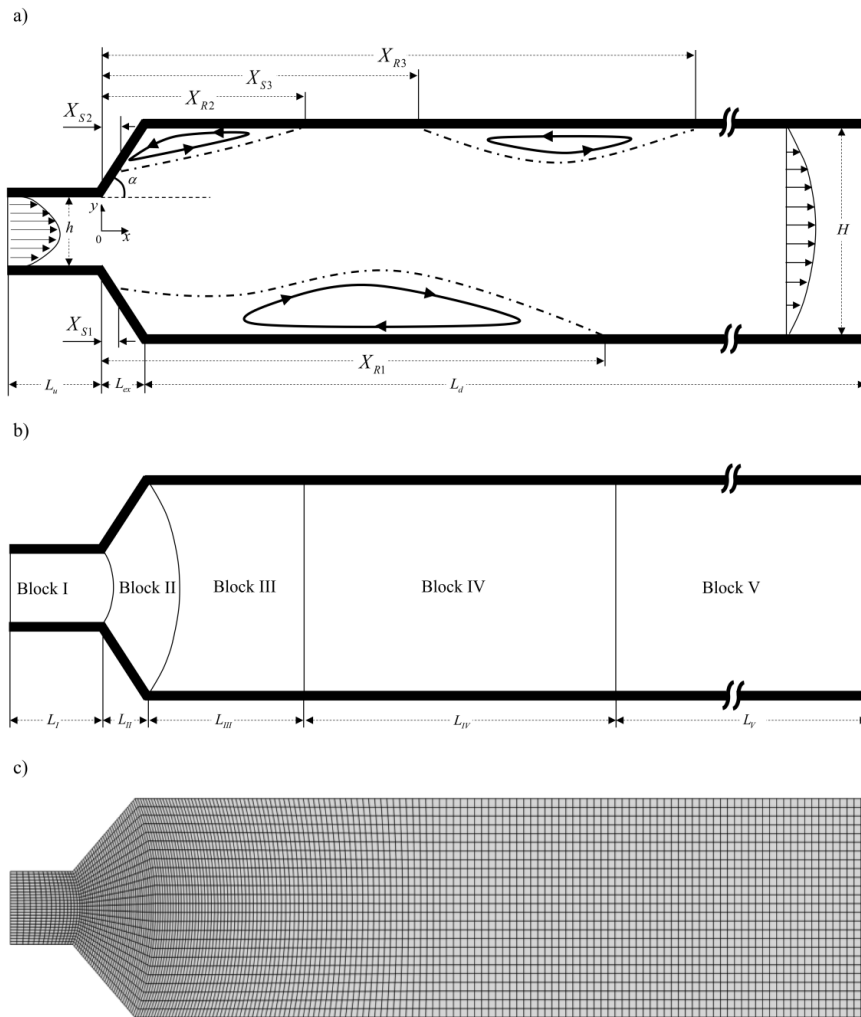


Fig. 1. Illustration of (a) two-dimensional 1:3 gradual planar expansion geometry considered in the study and (b) blocks that were used; (c) mesh distribution near the expansion plane (Mesh 1, $\alpha = 45^\circ$, $-1 < x/h < 13$ and $-1.5 < y/h < 1.5$).

opposite effect. *Norouzi et al. (2015)* studied numerically the flow of viscoelastic fluid through a 1:3 planar gradual expansion. Three angles of 30, 45, and 60° are selected to clarify the effect of expansion angles. The exponential Phan Thien-Tanner (EPTT) model is used as the constitutive equation. The results proved that an increase in expansion angles destabilizes the flow regime.

From the aforementioned discussion, it is clear that a comprehensive investigation on the flow of purely viscous non-Newtonian fluids in planar expansions is still lacking of an angle of expansion below 90° (gradual expansions). The object of the present paper is to examine the details of the symmetric and asymmetric flow patterns obtained in the laminar steady flow of incompressible shear-thinning fluids through a 1:3 planar gradual expansions. The non-Newtonian fluids used follow the Power-Law model ($n = 0.6$ and 0.8) and are compared to the Newtonian fluid ($n = 1.0$). In order to evaluate the effect of gradual expansion angles α , four angles including 15, 30, 45 and 60° are selected, and are compared to a sudden expansion ($\alpha = 90^\circ$). The

effect of generalized Reynolds number is examined in the range of 1 - 400.

2. MATHEMATICAL FORMULATION

2.1. Problem Description

The shear-thinning fluid flow in a 1:3 planar gradual expansion was considered as depicted in Fig. 1(a). According to the figure, the lengths and heights of the upstream and downstream sections relating to the first and third parts are respectively represented as L_u , h , L_d and H . The length and the expansion angle of the second part are denoted as L_{ex} and α , where $H/h = 3$, $L_u = h$, $L_{ex} = h / \tan(\alpha)$ and $L_d = 75h - L_{ex}$. To ensure that the length of the channel is large enough for fully-developed flow to establish itself at the exit (outlet), a comparison of numerical profiles with the analytical one for the three "n" tried and for three angles of expansion (90°, 45° and 15°) is presented in Fig. 2(b). This figure shows an excellent agreement between numerical and analytical

profiles, which confirms that the channel length is sufficient.

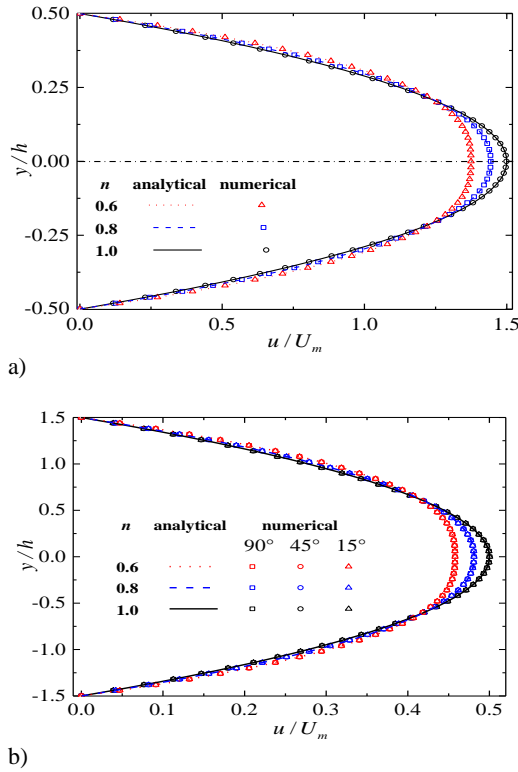


Fig. 2. Analytical and numerical fully-developed velocity profiles at $Re_g = 200$ and for $n = 0.6, 0.8$ and 1.0 : a) inlet and b) outlet.

2.2. Governing Equations

The flow is considered laminar, steady and incompressible and the fluid in the planar expansion flows in the positive x-direction. This 2D flow is governed by the continuity equation

$$\frac{\partial u}{\partial x} + \frac{\partial v}{\partial y} = 0 \quad (1)$$

and the momentum equations:

$$\rho \left(u \frac{\partial u}{\partial x} + v \frac{\partial u}{\partial y} \right) = -\frac{\partial P}{\partial x} + \left(\frac{\partial \tau_{xx}}{\partial x} + \frac{\partial \tau_{xy}}{\partial y} \right) \quad (2)$$

$$\rho \left(u \frac{\partial v}{\partial x} + v \frac{\partial v}{\partial y} \right) = -\frac{\partial P}{\partial y} + \left(\frac{\partial \tau_{xy}}{\partial x} + \frac{\partial \tau_{yy}}{\partial y} \right) \quad (3)$$

The Power-Law model is used, and the extra-stress tensor is calculated as

$$\tau_{ij} = 2\eta(\dot{\gamma})D_{ij} \quad (4)$$

and D_{ij} is the rate of deformation tensor

$$D_{ij} = \frac{1}{2} \left(\frac{\partial u_i}{\partial x_j} + \frac{\partial u_j}{\partial x_i} \right) \quad (5)$$

The viscosity function follows the Power-Law model and is calculated as

$$\eta(\dot{\gamma}) = K \dot{\gamma}^{n-1} \quad (6)$$

Where K is the consistency index, n is the Power-Law exponent and $\dot{\gamma}$ is the effective shear rate which is related to the second invariant of the rate of deformation tensor (D_{ij}) by

$$\dot{\gamma} = \sqrt{2D:D} = \sqrt{2 \left(\frac{\partial u}{\partial x} \right)^2 + 2 \left(\frac{\partial v}{\partial y} \right)^2 + \left(\frac{\partial u}{\partial y} + \frac{\partial v}{\partial x} \right)^2} \quad (7)$$

Generalized Reynolds number used in this work obeying the relation of Metzner and Reed (1955) and is defined as

$$Re_g = \frac{6\rho(U_m)^{2-n} h^n}{K [(4n+2)/n]^n} \quad (8)$$

3. NUMERICAL PROCEDURE AND VALIDATION

The governing Eqs. (1) - (3) are solved using the software ANSYS Fluent 16.0, which employs the finite volume method. The Semi-Implicit Method for the Pressure-Linked Equations (SIMPLE) algorithm was used for solving the pressure-velocity coupling. To discretize the convective terms, Quadratic upwind differencing scheme (QUICK) was used and the central difference scheme used to discretize diffusive terms. The absolute residual values of the continuity, x-velocity and y-velocity are set at 10^{-6} , 10^{-8} and 10^{-8} respectively.

3.1. Boundary Conditions

The different boundary conditions used in this study are:

- At the entrance, the boundary condition is set to be velocity inlet with a fully-developed velocity profile and for the laminar flow of Power-Law fluids in a channel is given by Bird *et al.* (2002) as:

$$u(y) = U_m \left(\frac{2n+1}{n+1} \right) \left[1 - \left(\frac{y}{h/2} \right)^{(n+1)/n} \right] \quad (9)$$

This boundary condition is introduced in ANSYS Fluent 16.0, using a User-Defined Function (UDF). A comparison of the analytical and numerical velocity profile at the inlet of the expansion at $Re_g = 200$ for different Power-Law index n (0.6, 0.8 and 1.0) as shown in Fig. 2(a). The results show an excellent agreement between analytical and numerical profile. This confirms that the UDF elaborated in this study gives a good result. It is noted that the decrease of the Power-Law index flattens the velocity profile near the center of the channel.

- At the outlet, the boundary condition is set to pressure outlet (atmospheric pressure).

Table 1 Computational domain and mesh characteristics of the 1:3 planar expansions geometry

Block	N _x					N _y	R _x	R _y	N _c				
	α=90°	α=60°	α=45°	α=30°	α=15°				α=90°	α=60°	α=45°	α=30°	α=15°
M1													
block I	16	16	16	16	16	26	0.935	1	375	375	375	375	375
block II	26	30	36	51	98	26	1	1	625	725	875	1250	2425
block III	71	71	71	71	71	26	1.0145	1	1750	1750	1750	1750	1750
block IV	267	267	267	267	267	26	1	1	6650	6650	6650	6650	6650
block V	71	71	71	71	71	26	1.0394	1	1750	1750	1750	1750	1750
N _{c,total}									11150	11250	11400	11775	12950
M2													
block I	31	31	31	31	31	51	0.9675	1	1500	1500	1500	1500	1500
block II	51	59	71	101	195	51	1	1	2500	2900	3500	5000	9700
block III	141	141	141	141	141	51	1.0072	1	7000	7000	7000	7000	7000
block IV	533	533	533	533	533	51	1	1	26600	26600	26600	26600	26600
block V	141	141	141	141	141	51	1.0197	1	7000	7000	7000	7000	7000
N _{c,total}									44600	45000	45600	47100	51800
M3													
block I	61	61	61	61	61	101	0.9837	1	6000	6000	6000	6000	6000
block II	101	117	141	201	389	101	1	1	10000	11600	14000	20000	38800
block III	281	281	281	281	281	101	1.0036	1	28000	28000	28000	28000	28000
block IV	1065	1065	1065	1065	1065	101	1	1	106400	106400	106400	106400	106400
block V	281	281	281	281	281	101	1.0098	1	28000	28000	28000	28000	28000
N _{c,total}									178400	180000	182400	188400	207200

- Along the walls of the channel, no-slip condition is imposed for the fluid velocity.

3.2. Grid-Independency Study

The grid independence of the results has been established on the basis of a detailed analysis of three different meshes: fine, medium and coarse (Table 1). For the general primitive variable ϕ (separation and reattachment lengths) the grid-converged value (i.e. extrapolated to the zero element size), according to Richardson extrapolation (Roache, 1997) is given as

$$\phi_{ext} = \phi_{M3} - \frac{(\phi_{M2} - \phi_{M3})}{(r^p - 1)} \quad (10)$$

Where ϕ_{M3} is obtained based on the finest grid, ϕ_{M2} is the solution based on the next level of coarse grid, $r = 2$ is the ratio between the coarse and fine grid spacing and p is the actual order of accuracy, where p is calculated with the following equation

$$p = \frac{\ln\left(\frac{\phi_{M3} - \phi_{M2}}{\phi_{M2} - \phi_{M1}}\right)}{\ln(r)} \quad (11)$$

The grid size effect on the dimensionless output parameters such as the lengths of reattachment and separation (X_{R1} , X_{R2} , X_{R3} and X_{S3}) was tested at three grid structures (symbolically represented as $M1$, $M2$ and $M3$ with $\Delta x_{min} / h = \Delta y_{min} / h = 0.04$, 0.02 and 0.01 respectively). Three generalized Reynolds number ($Re_g = 360$, $Re_g = 280$ and $Re_g = 200$ for $n = 0.6$, 0.8 and 1.0 respectively) and two

expansion angles (90° and 15°) were considered (Table 2).

The value of Er given in Table 2 is a quantification of the relative difference between the separation and reattachment lengths calculated with $M2$ and that extrapolated.

The maximum relative error in Table 2 was found to be about 3% at $n = 0.6$, $Re_g = 360$ and $\alpha = 90^\circ$ for X_{S3} , this error reduces to about 2% when the expansion angle reduces to 15° . For $n = 1.0$, $Re_g = 200$ and $\alpha = 90^\circ$, the maximum relative error of X_{S3} was found to be about 1.7% and reduces to about 1.3% when the expansion angle reduces to 15° . As seen in Table 2, results for $M2$ and $M3$ are close to each other. Due to larger CPU time and computational cost of $M3$ especially when Re_g is close to the two critical values, mesh $M2$ denotes a good compromise between the accuracy and computational efforts and hence all results reported herein are based on the use of mesh $M2$.

3.3. Validation

In Fig. 3 the comparison of streamwise velocity profile of our numerical calculations for Newtonian fluid ($n = 1.0$) with the experimental values obtained in the work of Fearn *et al.* (1990) is presented. Three generalized Reynolds numbers are tested 34.7, 80 and 186.7, corresponding to: two symmetric vortices, two vortices of unequal size and three vortices respectively. An excellent agreement with the results of Fearn *et al.* (1990) can be observed. We note that in the results of Fearn *et al.* (1990) the values of these three Reynolds

Table 2 Mesh dependency tests for $\alpha = 90^\circ$ and 15°

Mesh	$\alpha = 90^\circ$				$\alpha = 15^\circ$			
	X_{R1}	X_{R2}	X_{S3}	X_{R3}	X_{R1}	X_{R2}	X_{S3}	X_{R3}
$n = 0.6$ and $Re_g = 360$								
$M1$	17,9336	4,6771	15,4343	25,8221	18,9735	4,5594	16,9332	24,5262
$M2$	19,8004	5,1587	17,3618	26,7936	19,8617	4,6669	18,1306	24,4165
$M3$	20,1927	5,2686	17,8060	26,8736	20,0466	4,6874	18,4244	24,3230
Extrapolated	20,2971	5,3011	17,9390	26,8808	20,0952	4,6922	18,5199	23,7834
Er (%)	2,4470	2,6861	3,2177	0,3243	1,1620	0,5398	2,1022	2,6621
$n = 0.8$ and $Re_g = 280$								
$M1$	16,3530	4,5425	13,5150	27,4222	17,6100	4,4066	14,8478	26,5802
$M2$	17,8900	4,9116	14,9962	28,5642	18,5375	4,4881	15,8010	26,8235
$M3$	18,1722	4,9840	15,2808	28,7052	18,7302	4,5035	16,0096	26,8242
Extrapolated	18,2357	5,0017	15,3485	28,7251	18,7807	4,5071	16,0680	26,8242
Er (%)	1,8955	1,8007	2,2953	0,5600	1,2951	0,4213	1,6619	0,0026
$n = 1.0$ and $Re_g = 200$								
$M1$	14,5267	4,3051	11,6985	26,3726	15,7988	4,1874	12,9551	25,7068
$M2$	15,5840	4,5662	12,6757	27,3675	16,4739	4,2479	13,6112	25,9772
$M3$	15,7670	4,6128	12,8548	27,4997	16,6133	4,2600	13,7542	25,9947
Extrapolated	15,8053	4,6229	12,8950	27,5200	16,6496	4,2630	13,7941	25,9959
Er (%)	1,4002	1,2270	1,7006	0,5540	1,0551	0,3548	1,3256	0,0720

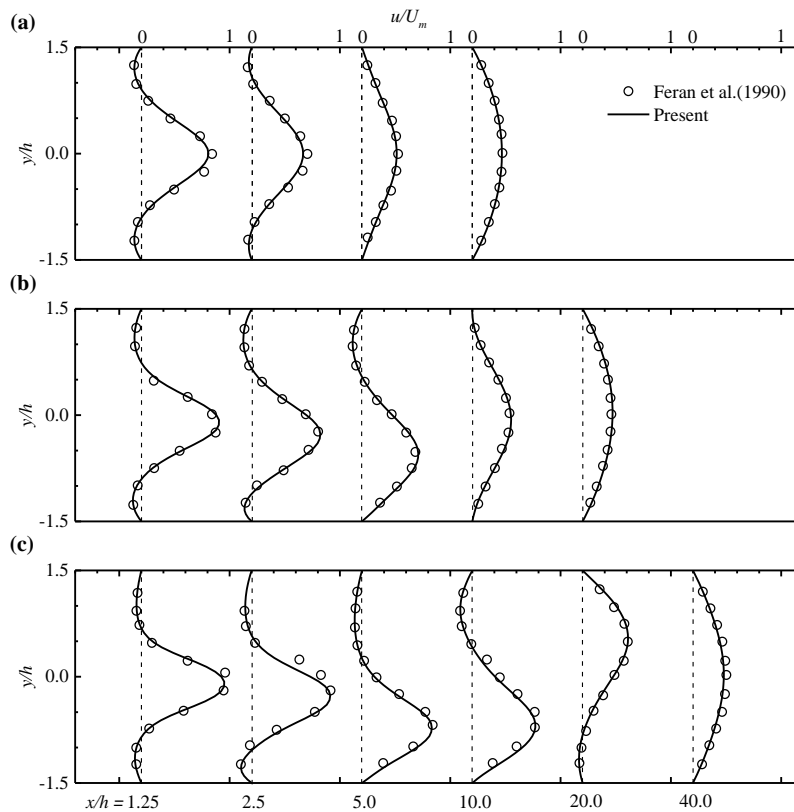


Fig. 3. Comparison of the streamwise velocity profile between numerical results (present work) and experimental results (Fearn *et al.*, 1990) at $n = 1.0$: (a) $Re_g = 34.7$, (b) $Re_g = 80$ and (c) $Re_g = 186.7$.

Table 3 Comparison between works concerned with the phenomenon of sudden-expansion flow asymmetry for Newtonian and non-Newtonian fluids

Author	Definition of Re	Re_{ger1}	$Re_{ger1}(U_m, h)$	$Re_{ger2}(U_m, h)$
Newtonian ($n=1.0$)				
Fearn <i>et al.</i> (1990)	$U_{max}, h/2$	40.5	53.9	-
Foumeny <i>et al.</i> (1996)	U_{max}, h	≈ 80	≈ 53.3	-
Battaglia <i>et al.</i> (1997)	U_m, h	53.8	53.8	-
Drikakis (1997)	U_{max}, h	80	53.3	-
Schreck and Schäfer (2000)	U_{max}, h	81.2	54.1	-
Ternik (2009)	U_m, h	54	54	103.9
Dhinakaran <i>et al.</i> (2013)	U_m, h	54.5	54.5	102.2
Present work	U_m, h	54.4	54.4	99.4
Power law ($n=0.8$)				
Ternik (2009)	U_m, h	76	76	-
Dhinakaran <i>et al.</i> (2013)	U_m, h	74.1	74.1	158.3
Present work	U_m, h	78.1	78.1	152.1
Power law ($n=0.6$)				
Ternik (2009)	U_m, h	110	110	-
Dhinakaran <i>et al.</i> (2013)	U_m, h	≈ 110	≈ 110	≈ 252
Present work	U_m, h	113.1	113.1	246.9

numbers are 26, 60 and 140 respectively (when the Reynolds number is based on the upstream expansion half-height and the maximum inlet velocity).

For $Re_g = 34.7$ and for the four positions (Fig. 3(a)) the profile remain symmetric about the centerline. The results show that after $x/h = 4$, the two recirculation zones have no effect on the velocity profile which becomes parabolic again from $x/h = 10$. At a Reynolds number of 80 (Fig. 3(b)), the flow remains asymmetric until $x/h = 10$ where it is again symmetric and at $x/h = 21.82$ the velocity profile is once again parabolic. For $Re_g = 186.7$ (Fig. 3(c)), we observe the existence of a third recirculation zone between $x/h = 12.36$ and 25.80 whereas from $x/h = 52.06$ the velocity has recovered its parabolic profile.

Most authors cited in this paper explained the asymmetric flow phenomenon by the Coanda effect (Fearn *et al.*, 1990; Oliveira 2003; Ternik *et al.* 2006; Dhinakaran *et al.* 2013 and Norouzi *et al.* 2015), where any perturbation of the flow field, pushing the main flow to one of the sides of the expansion, gives rise to larger velocities and lower pressures there, and hence the asymmetry (i.e. two vortices of unequal size) will naturally tend to be accentuated Oliveira (2003). It is also worthwhile pointing out that the appearance of the larger vortex on either the upper or the lower wall is purely random (Neofytou and Drikakis, 2003; Oliveira 2003; Ternik *et al.*, 2006 and Foumeny *et al.*, 1996).

Table 3 presents a comparison between the values of critical generalized Reynolds numbers obtained in this study and those obtained by certain authors. For this comparison, columns 4 and 5 give the converted values of Re_{ger} (respectively $Re_{ger1}(U_m, h)$ and $Re_{ger2}(U_m, h)$). This conversion is done to make the generalized Reynolds number based on the mean velocity U_m and the height h at the inlet of the expansion. For the different values of n , the critical generalized Reynolds numbers obtained in this study are very close to those of the works reported in the literature.

4. RESULTS AND DISCUSSION

In this section, we present a detailed analysis of the results concerning the effects of expansion angle and shear-thinning behaviour on the vortices characteristics obtained for a generalized Reynolds number ranging from 1 to 400.

The Figs. 4(a–c) show an excellent agreement between our predictions and those of Ternik (2009) and Dhinakaran *et al.* (2013). This also includes bifurcations observed in these figures where its appearance depends on the generalized Reynolds number and the Power-Law index. Figure 4(a) displays the variation of the lengths of the upper and lower recirculation zones with the generalized Reynolds number at $n=1$ (Newtonian fluid). For $Re_g < Re_{ger1}$ ($Re_{ger1} = 54.4$) the flow remains steady and symmetric (i.e. $X_{R1} = X_{R2}$). The length of recirculation zones grow linearly with Re_g ,

when Re_g exceeding this critical value the flow becomes asymmetric (i.e. $X_{R1} \neq X_{R2}$) and the length of the lower recirculation zone continues to increase conversely the upper recirculation zone continues to decrease up to $Re_g \approx 80$. Beyond this value, X_{R1} continues to increase while X_{R2} varies slightly up to $Re_g = 99.4$ (Re_{gcr2}). This value of Re_g corresponds to the apparition of a third recirculation zone in the downstream of the smallest recirculation zone. For $Re_g > Re_{gcr2}$, the third recirculation zone starts to grow and the two other vortices continue to increase. Noting that the growth of X_{R1} and X_{R3} is more intensive than X_{R2} and X_{S3} . These remarks were also observed for Figs. 4(b) and 4(c). Comparing these two figures with Fig. 4(a), we notice that for the shear-thinning fluids ($n=0.8$ and $n=0.6$) the two flow transitions are delayed due to the decreases of the flow sensitivity to the perturbation as the shear-thinning behaviour is enhanced (n decreases). This is also attested by Ternik (2009) and Dhinakaran *et al.* (2013). The values of the critical generalized Reynolds numbers for shear-thinning-fluids are given in Table 3.

Figure 5 illustrates the influence of the shear-thinning behaviour on the separation and reattachment lengths of the recirculation zones for different expansion angles. This figure shows that the decrease of Power-Law index delays the flow transition regardless of the expansion angle and affects the vortices characteristics.

It is noted that for the same generalized Reynolds number, the distance x/h from which there is no recirculation zone decreases with the decrease of the Power-Law index. This is due to the reduction in the fluid viscosity (shear-thinning) when the power law index decreases. This result is similar for all expansion angles.

To observe the effect of expansion angle on the separation and reattachment lengths of the recirculation zones, these lengths are plotted as a function of the generalized Reynolds number for different expansion angles and for the same Power-Law index (Fig. 6). This figure shows that the decrease of the expansion angle delays both the transition from symmetric to asymmetric flow and the apparition of the third recirculation zone. This result is valid for the three Power-Law indices used in this study.

From Figs. (5) and (6) one can see that the difference between the two critical generalized Reynolds numbers ΔRe_{gcr} increases with either the decrease in the Power-Law index or the decrease in the expansion angle. For the different expansion angles and Power-Law indices used, one can note that the generalized Reynolds number has no influence on the length X_{R2} from certain values.

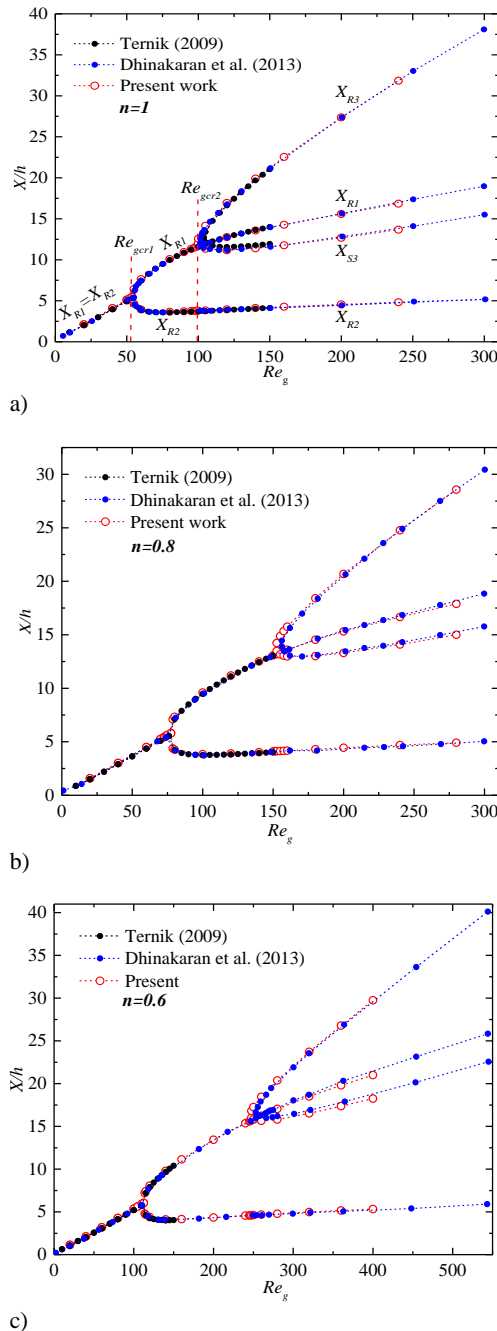


Fig. 4. Variation of vortex size with generalized Reynolds number for the Power-Law fluid flow in a 1:3 planar sudden expansion ($\alpha = 90^\circ$), and comparison with the available literature data: a) $n = 1.0$; b) $n = 0.8$ and c) $n = 0.6$.

The variation of pressure gradient with axial distance for Newtonian and non-Newtonian fluids is depicted in Fig. 7 for different expansion angles at two Re_g (100, 200). This variation is presented by a plot of the dimensionless pressure drop (normalized by the dynamic pressure $0.5\rho U_m^2$) along the centerline (from entrance to exit).

In an upstream region, the pressure drop is linear indicating fully-developed flow conditions for both Newtonian and shear-thinning fluids. As the fluid

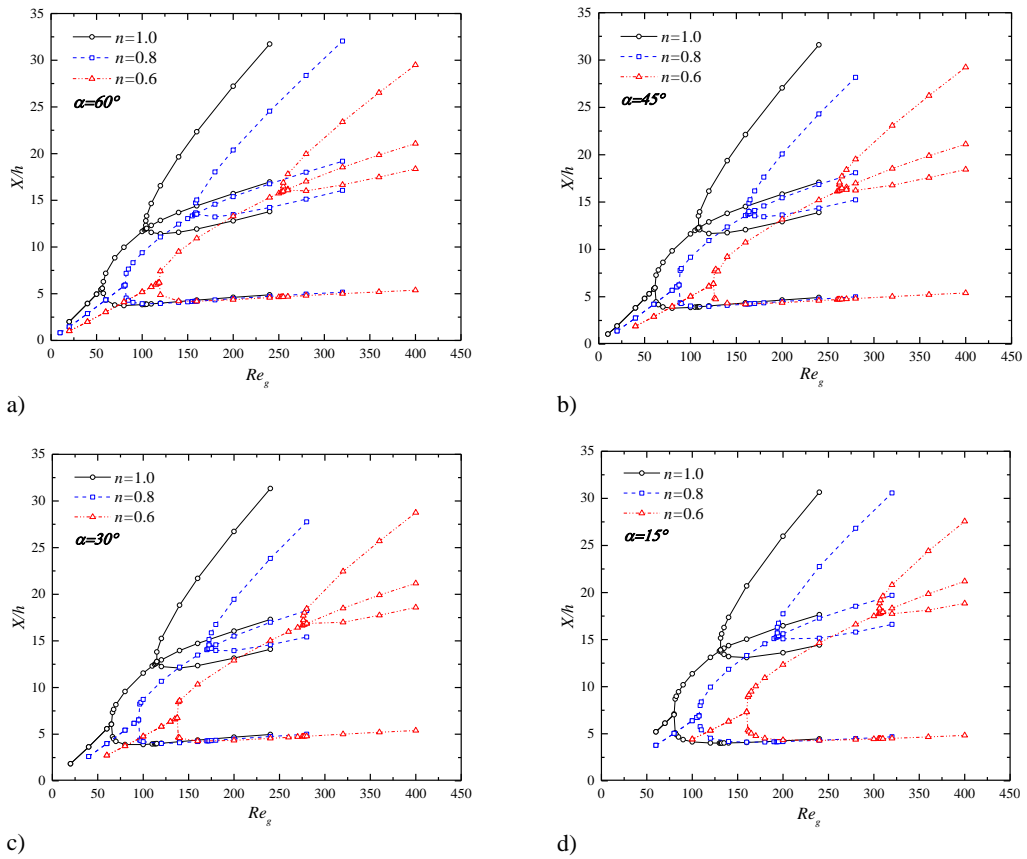


Fig. 5. Variation of vortex size with Re_g for $n = 1.0, 0.8$ and 0.6 , at different expansion angles:

a) $\alpha = 60^\circ$, b) $\alpha = 45^\circ$, c) $\alpha = 30^\circ$ and d) $\alpha = 15^\circ$.

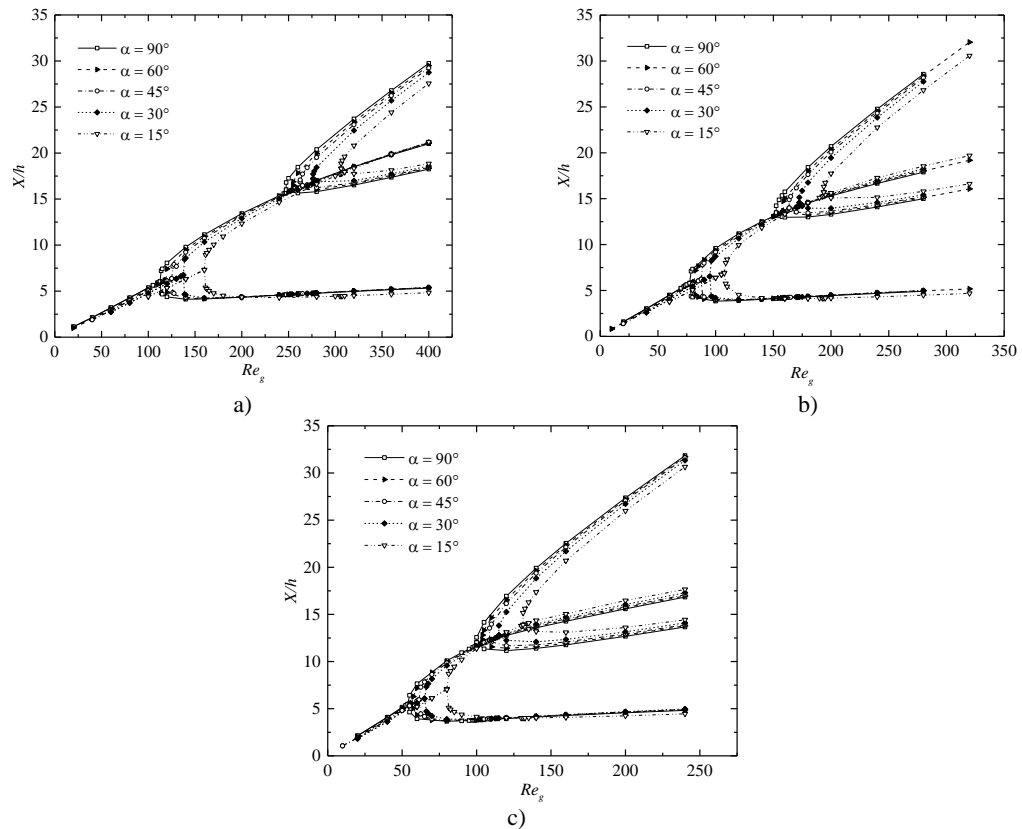


Fig. 6. Variation of vortex size with Re_g at different expansion angles for different Power-Law indices:

a) $n = 0.6$, b) $n = 0.8$ and c) $n = 1.0$.

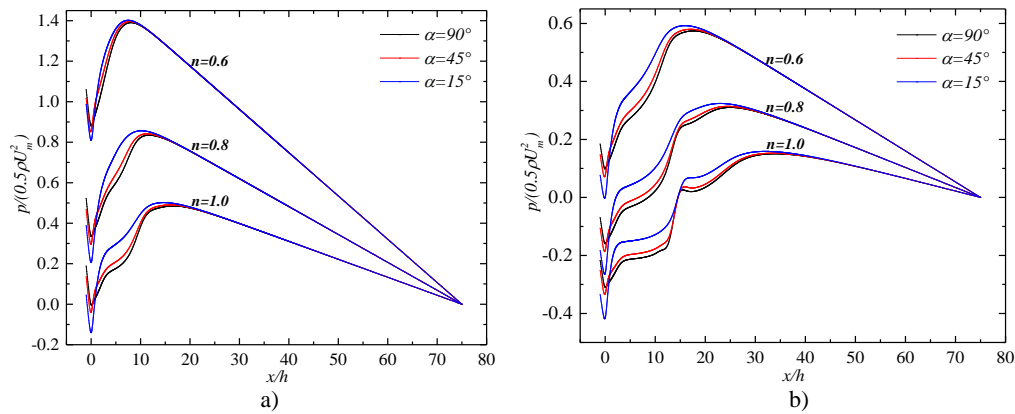


Fig. 7. Normalized pressure variation along the channel centerline: a) $Re_g = 100$ and b) $Re_g = 200$.

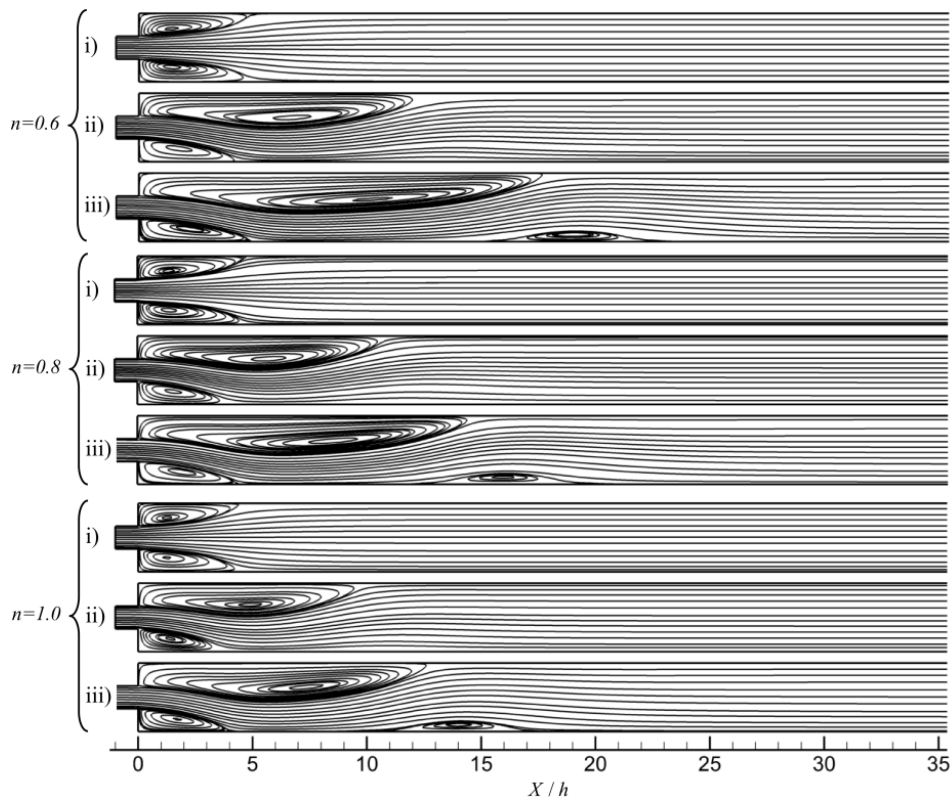


Fig. 8. Flow patterns in the 1:3 planar sudden expansion ($\alpha = 90^\circ$) at different Power-Law index values: $n = 0.6$, $n = 0.8$ and $n = 1.0$.

flow passes the expansion plane ($x/h \geq 0$), the local pressure increases because of the flow deceleration through the downstream section. Subsequently, the pressure distribution returns to the linear variation within the downstream section of expansion. For the flow at higher Re_g , the pressure variation is more complex and reflects the different reattachment lengths of the smaller and the larger asymmetric vortices (inflection seen in the curves) (Oliveira 2003 and Ternik 2009).

In comparison to a Newtonian fluid, the pressure distribution for the shear-thinning fluid has larger gradients. The pressure recovery after the expansion is lower when the shear-thinning behaviour is enhanced.

For the same flow index, the increase in the critical Reynolds number when the expansion angle is decreased is due to the change in pressure. Indeed, the reduction in the expansion angle causes a progressive decrease in cross-section and therefore a gradual increase in pressure, which stabilizes the flow.

To illustrate the effect of shear-thinning and expansion angle on the flow patterns, the plots of streamline are presented in Figs. 8, 9 and 10 for different expansion angles 90° , 45° and 15° respectively. For all these figures, the streamline is plotted at three Power-Law indices n for three different regimes. These regimes are chosen as those chosen by Dhinakaran *et al.* (2013) and they

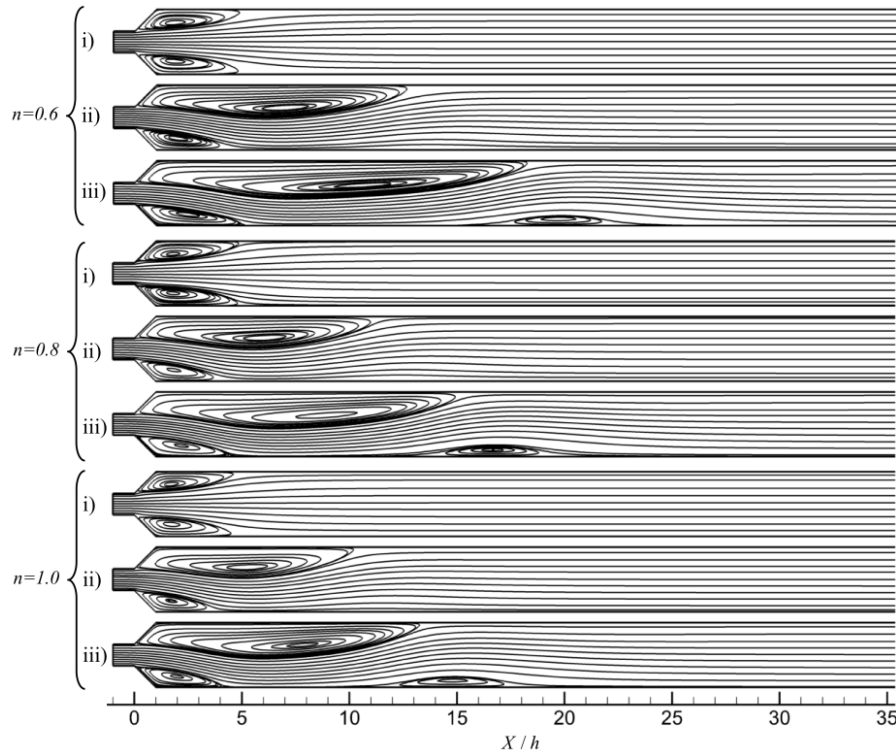


Fig. 9. Flow patterns in the 1:3 planar gradual expansion ($\alpha = 45^\circ$) at different Power-Law index values: $n = 0.6$, $n = 0.8$ and $n = 1.0$.

are: i) symmetric flow ($Re_g = 0.8Re_{gcr1}$), ii) asymmetric flow [$Re_g = 0.5(Re_{gcr1} + Re_{gcr2})$] and iii) asymmetric flow with a third recirculating zone ($Re_g = 1.2Re_{gcr2}$). Since there is a strong variation of the two critical generalized Reynolds number values with n .

For the sudden expansion $\alpha = 90^\circ$ (Fig. 8), it is visible that for the three aforementioned regimes, the three vortices lengths increase within the Power-Law index decrease. The same observation is valid for the gradual expansions with expansion angles of $\alpha = 45^\circ$ and $\alpha = 15^\circ$ (Figs. 9 and 10). Comparing the Figs. 8, 9 and 10, we can observe that the decrease of the expansion angle increases the lengths of all vortices. One can see also that the width of the small corner recirculation zone decreases in the case of regime iii) both with the decrease of the expansion angle or with the increase of the Power-Law index.

In order to determine the correlations of the two critical generalized Reynolds numbers as a function of n and α , a modification taking into account the effect of the expansion angle was made on the two models of Dhinakaran *et al.* (2013) developed for a sudden expansion. These two correlations (Eqs. (12) and (13)) are derived on the basis of calculated numerical data for Re_{gcr1} and Re_{gcr2} .

$$Re_{gcr1} = \frac{112 + 92e^{-0.038\alpha}}{\sinh(1.5n)} + \frac{1}{\cosh(0.5n)} \quad (12)$$

$$Re_{gcr2} = \frac{565 + 162e^{-0.046\alpha}}{\sinh(3n)} + \frac{66 + 74.5e^{-0.048\alpha}}{\cosh(n)} \quad (13)$$

The comparison between numerical data and the two models is presented in Fig. 11, where the maximum error obtained is 3.2% and 1.24% for Eq. (12) and Eq. (13) respectively.

The Fig. 11 shows also the variation of the two critical generalized Reynolds numbers Re_{gcr1} and Re_{gcr2} as a function of n and α . In this figure and as already pointed out, the decrease of the Power-Law index or the expansion angle stabilizes the flow by increasing significantly the two critical generalized Reynolds numbers. Thus, one can see that the variation of Re_{gcr2} as a function of n is faster than that of Re_{gcr1} .

The results obtained previously showed the effect of Power-Law index and expansion angle on the flow pattern (recirculation zones), but no indication of the values of Reynolds number from which these zones appear ($Re_{g,RA}$). Table 4 shows the value of

$Re_{g,RA}$ as a function of the Power-Law index and the expansion angle. This value increases either when the Power-Law index or the expansion angle decreases. The results obtained in this study show that for the 90° expansion angle the flow is always accompanied by a recirculation zones. This result is similar to that found by Dhinakaran *et al.* (2013) and Ternik (2010), who found that these zones are present even for very low values of generalized Reynolds number (up to 0.01).

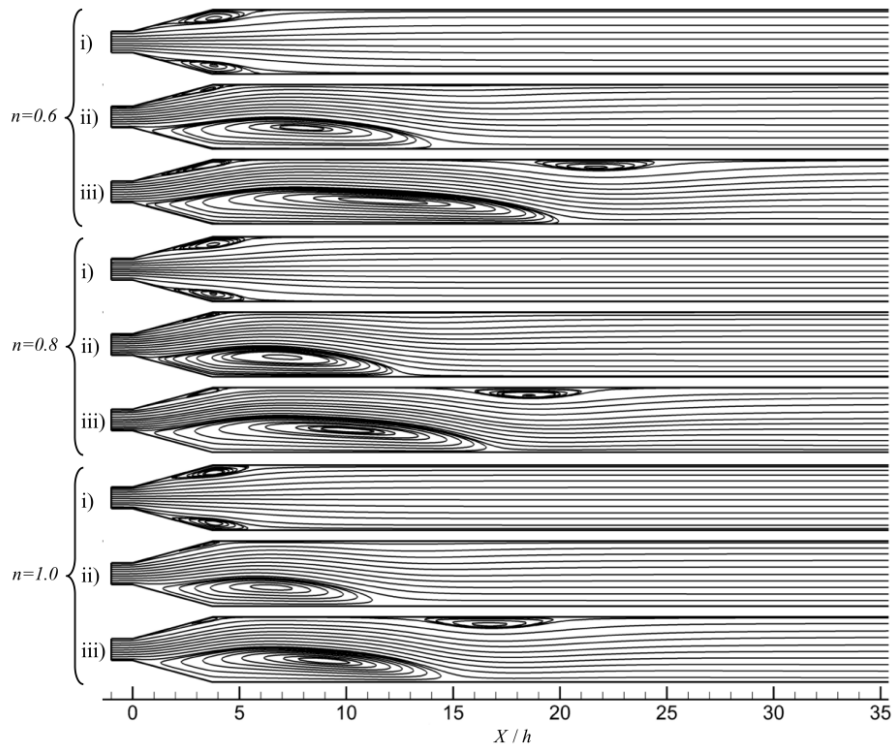


Fig. 10. Flow patterns in the 1:3 planar gradual expansion ($\alpha = 15^\circ$) at different Power-Law indices values: $n = 0.6$, $n = 0.8$ and $n = 1.0$.

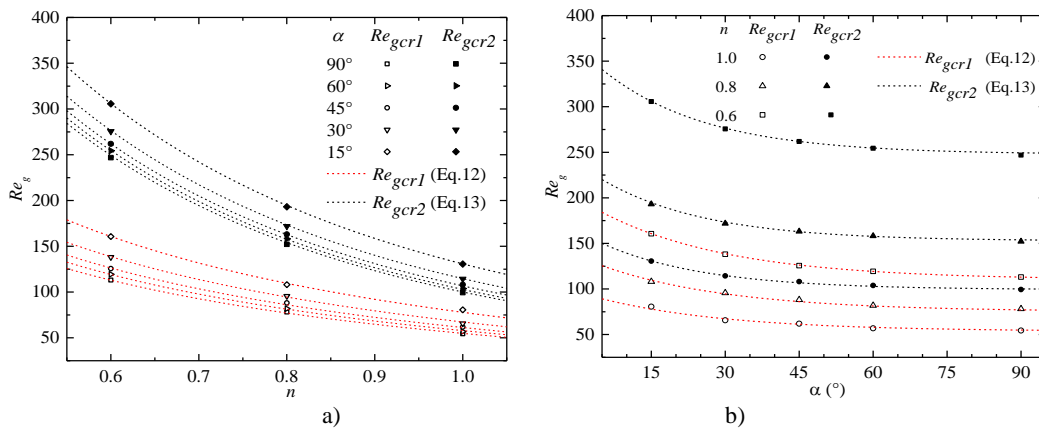


Fig. 11. Effect of Power-Law index (n) and expansion angle (α) on the two critical generalized Reynolds numbers: **a)** $Re_{gcr} = f(n)$, **b)** $Re_{gcr} = f(\alpha)$.

Table 4 Comparison of the $Re_{g,RA}$ values for different expansion angle and Power-Law index

$\alpha(^{\circ})$	$Re_{g,RA}$			
	60	45	30	15
$n = 1.0$	1.88	9.38	19.38	43.13
$n = 0.8$	5.63	14.38	27.13	59.38
$n = 0.6$	10.63	23.13	40.63	85.63

5. CONCLUSIONS AND PERSPECTIVES

In the present study, laminar 2-D incompressible

flow of shear-thinning fluid through a planar gradual expansion is investigated numerically. non-Newtonian Power-Law model is used for the problem simulations. Variation of different parameters such as Power-Law index n , expansion angle α and generalized Reynolds number Re_g are studied. The results indicate a great dependence of the problem flow pattern with these parameters and some of the results are pointed below:

* The decrease of the Power-Law index or the expansion angle stabilizes the flow by significantly increasing the two critical generalized Reynolds numbers, and this is due to the decrease of the transverse pressure gradient.

* The value of generalized Reynolds number from which the recirculation zone appears increases when the Power-Law index or the expansion angle is decreased. For a sudden expansion, the flow is always accompanied by a recirculation zones.

Research perspectives in this field include the detection of the bifurcation points for shear-thickening fluids and the verification of the validity of the tow proposed correlations. On the other hand, study the effect of channel depth on the tow critical Reynolds numbers (3D study).

ACKNOWLEDGEMENTS

The authors would like to acknowledge the assistance of the staffs of the laboratory of Industrial Technologies at Ibn Khaldoun University -Tiaret and the Smart Structures Laboratory at the University center of Ain Témouchent, Algeria.

REFERENCES

- Battaglia, F., S. J. Tavener, A. K. Kulkarni and C. L. Merkle (1997). Bifurcation of low Reynolds number flows in symmetric channels. *AIAA Journal* 35(1), 99-105.
- Bird, R. B., W. E. Stewart and E. N. Lightfoot (2002). *Transport Phenomena*. Second. J. Wiley.
- Cherdron, W., F. Durst and J. H. Whitelaw (1978). Asymmetric flows and instabilities in symmetric ducts with sudden expansions. *Journal of Fluid Mechanics* 84(1), 13-31.
- Chiang, T. P., T. W. Sheu and S. K. Wang (2000). Side wall effects on the structure of laminar flow over a plane-symmetric sudden expansion. *Computers & fluids* 29(5), 467-492.
- De Zilwa, S. R. N., L. Khezzar and J. H. Whitelaw (2000). Flows through plane sudden - expansions. *International Journal for Numerical Methods in Fluids* 32(3), 313-329.
- Dhinakaran, S., M. S. N. Oliveira, F. T. Pinho and M. A. Alves (2013). Steady flow of power-law fluids in a 1: 3 planar sudden expansion. *Journal of Non-Newtonian Fluid Mechanics* 198, 48-58.
- Drikakis, D. (1997). Bifurcation phenomena in incompressible sudden expansion flows. *Physics of Fluids* 9(1), 76-87.
- Durst, F., A. Melling and J. H. Whitelaw (1974). Low Reynolds number flow over a plane symmetric sudden expansion. *Journal of fluid mechanics* 64(1), 111-128.
- Fearn, R. M., T. Mullin and K. A. Cliffe (1990). Nonlinear flow phenomena in a symmetric sudden expansion. *Journal of Fluid Mechanics* 211, 595-608.
- Foumeny, E. A., D. B. Ingham & A. J. Walker (1996). Bifurcations of incompressible flow through plane symmetric channel expansions. *Computers & fluids* 25(3), 335-351.
- Jotkar, M., J. M. Pérez, V. Theofilis and R. Govindarajan (2015). Instability mechanisms in straight-diverging-straight channels. *Procedia IUTAM* 14, 236-245.
- Manica, R. and A. L. De Bortoli (2004). Simulation of sudden expansion flows for power-law fluids. *Journal of Non-Newtonian Fluid Mechanics* 121(1), 35-40.
- Metzner, A. B. and J. C. Reed (1955). Flow of non - newtonian fluids—correlation of the laminar, transition, and turbulent - flow regions. *Aiche journal*, 1(4), 434-440.
- Mishra, S. and K. Jayaraman (2002). Asymmetric flows in planar symmetric channels with large expansion ratio. *International journal for numerical methods in fluids* 38(10), 945-962.
- Neofytou, P. (2006). Transition to asymmetry of generalised Newtonian fluid flows through a symmetric sudden expansion. *Journal of non-newtonian fluid mechanics* 133(2-3), 132-140.
- Neofytou, P. and D. Drikakis (2003). Non-Newtonian flow instability in a channel with a sudden expansion. *Journal of Non-Newtonian Fluid Mechanics* 111(2-3), 127-150.
- Norouzi, M., M. M. Shahmardan and A. S. Zahiri (2015). Bifurcation phenomenon of inertial viscoelastic flow through gradual expansions. *Rheologica Acta* 54(5), 423-435.
- Oliveira, P. J. (2003). Asymmetric flows of viscoelastic fluids in symmetric planar expansion geometries. *Journal of non-newtonian fluid mechanics* 114(1), 33-63.
- Roache, P. J. (1997). Quantification of uncertainty in computational fluid dynamics. *Annual review of fluid Mechanics* 29(1), 123-160.
- Schreck, E. and M. Schäfer (2000). Numerical study of bifurcation in three-dimensional sudden channel expansions. *Computers & fluids* 29(5), 583-593.
- Ternik, P. (2009). Planar sudden symmetric expansion flows and bifurcation phenomena of purely viscous shear-thinning fluids. *Journal of non-newtonian fluid mechanics* 157(1-2), 15-25.
- Ternik, P. (2010). New contributions on laminar flow of inelastic non-Newtonian fluid in the two-dimensional symmetric expansion: Creeping and slowly moving flow conditions. *Journal of Non-Newtonian Fluid Mechanics* 165(19-20), 1400-1411.
- Ternik, P., J. Marn and Z. Žunič (2006). Non-Newtonian fluid flow through a planar symmetric expansion: Shear-thickening fluids. *Journal of non-newtonian fluid mechanics* 135(2-3), 136-148.

